A Kinematic Design of 3-PRS Precision Compliant Parallel Platform

Zhiping Kong[1, 2, a], Wei Zhang[1, 2, b], Haibo Zhou[1, 2, c]
[1]*School of Mechanical and Electrical Engineering, Central South University, Changsha, China*
[2]*State Key Laboratory of High Performance Complex Manufacturing, Central South University, Changsha, China*

Keywords: Parallel platform, Kinematics analysis, Large-stroke flexure joints.

Abstract: A kinematic design of the 3-PRS compliant parallel platform with wide-range flexure hinges is presented in this paper. The manipulator is driven by the piezoelectric motors, which can show the superiority of parallel platforms and large-stroke flexure hinges. First, taken into account the parasitic motions of the platform, the kinematics solution is proposed. Then, the influence of parameters to the rotation capacity and relative rotation error that are used to assess the quality of the revolute and spherical flexure joints. Also, the reachable travel is observed by ANSYS Workbench. Finally, compare with the FEM and the theoretical results by several different cases to ensure the efficiency of the kinematics model.

1 INTRODUCTION

High-precision positioning devices are often required in different areas as scientific, medical and communication fields for micro-system production (Ruiz, et al., 2016). For these high-tech applications, it is necessary to overcome the problems they usually appear, as clearances, friction and wear, which greatly affect the accuracy of the platform (Li and Xu, 2007). A well-known solution for these problems was put forward in (Bhagat U, et al., 2014), which introduced the compliant machines with the flexible hinges to improve the motion accuracy.

Parallel machine were first applied in the test of tire by Gough, and later were introduced by Stewart as the simulators (Stewart and D, 1965). Then the Stewart structure began to be widely used in many fields. Parallel manipulators with 6-DOF have many advantages. Dong et al established a kinematics model via analysing the stiffness model of the whole 6-PSS platform based on FEA method (Dong, et al., 2005). Recently, parallel platforms with less than 6-DOF have appeared in many different fields. Rouhani et al developed a method on the basis of elastokinematic analysis of a microhexapod manipulator, in which the elastic deformation of the flexure hinges was considered for the kinematic analysis (Rouhani, et al., 2016). Meanwhile, It is possible to develop 2-DOF mechanisms, as for example the stage presented in (Huang and Dao 2016), where the stage with flexure elements allows large displacement along x and y direction. Also, the paper provides some useful steps for designing and analyse by FEM. Many 3-DOF parallel manipulators also have been designed and applied for relevant areas. For example, the 3-UPU parallel robots with pure translational motions in (Gregorio, et al., 1998), other sample of this type is shown in (Liu, et al., 2005), where the parallel manipulator HANA has three DOF with one rotational and two translational degree of freedom. Another 3-DOF mechanism is presented in (Li,et al., 2005; Zhan, et al., 2005), where the kinematic of the 3-RPS parallel mechanism is analysed. Moreover, the necessary steps to achieve a good design and characterization are presented. Also 3-PUU mechanism with 2R1T is proposed in (Wang, et al., 2016), where the mobility analysis of the platform is carried out by the reciprocal screw theory.

The 3-PRS parallel platforms were widely designed and analysed in (Ruiz, et al., 2016; Li and Xu, 2007; Jia, et al., 2016; Li, et al., 2016; Tsai, et al., 2003). The 3-PRS parallel platform with large-stroke flexure joints introduced in this paper. At present, it is still a challenging task to solve the design and kinematic problem with flexible joints. For the mechanisms with flexible joints, they can overcome many problems, but they also faced some challenge, like the deformation of the joints and the parasitic motions. Therefore, it is necessary to study the design, kinematics and validate these compliant parallel platform with flexible joints.

Kong, Z., Zhang, W. and Zhou, H.
A Kinematic Design of 3-PRS Precision Compliant Parallel Platform.
DOI: 10.5220/0008849403410346
In *Proceedings of 5th International Conference on Vehicle, Mechanical and Electrical Engineering (ICVMEE 2019)*, pages 341-346
ISBN: 978-989-758-412-1

The present will develop the conceptual design, kinematics study, FEM validation of the 3- PRS parallel mechanism. Firstly, the design of the 3-PRS parallel platform are presented in Section 2. Then the kinematics are analysed in Sections 3, where the rigid body kinematics of the 3-PRS will be developed. The FEM of the large-stroke joints will be explained in section 4, where the kinematics simulation are concluded. Finally, some concluding remarks are given in Section 5.

2 SYSTEM DESCRIPTION

The structure of a 3-PRS parallel manipulator is composed of a moving platform, a fixed base, and three identical supporting limbs, which is shown in Figure 1. Each kinematic limb consists of two wide-range flexure hinges and a rigid rod in the middle. As shown in Fig.1, one wide-range flexure hinges is spherical joint (S) that can rotate around three axes, another is revolute joint (R) that can rotate around one axe. They can not only have high accuracy, but also achieve a long strike motion for parallel platform. The driving components as active joint (P), and a piezoelectric motor is utilized as actuator, which has many advantages as high precision, high driving force and large travel. Here, beryllium bronze and duralumin are used as the material of the long-stroke flexible joints and the others.

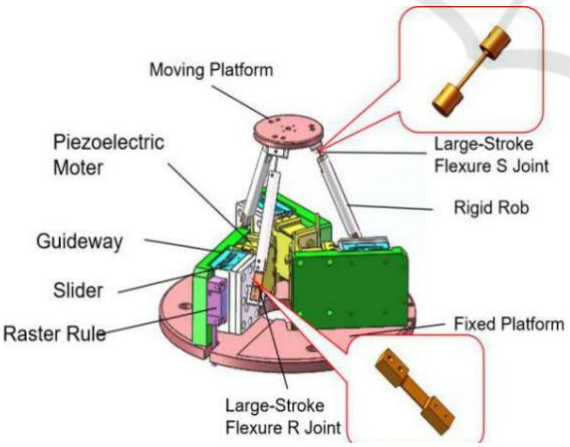

Figure 1. Basic configuration of the 3-PRS parallel manipulator.

The main parameters of the platform are obtained, as shown in Table1.

Table 1. The structure parameters of the 3-PRS parallel manipulator.

Item	Value
Diameter of moving platform	50mm
Angle between the kinematic chain and the fixed platform	65 °
Length of rigid rod	76mm
Diameter of rigid rod	10mm
chamfering radius of S joint and R joint	1mm
Diameter of S joint	1mm
Length of S joint and R joint	12mm
Thickness of R joint	0.4mm
Width of R joint	8mm

3 KINEMATICS ANALYSIS

The structure of the 3-PRS parallel mechanism is shown in Figure 2. Three coordinate systems are considered: the local coordinate systems P(xyz) in the center of the moving platform; and the global coordinate systems O(xyz) in the center of the fixed platform. The position of the center of the moving platform can be expressed by px , py and pz, and its direction can be represented by the angles α, β, and γ, which are the rotation angle around the x, y and z axes, respectively..

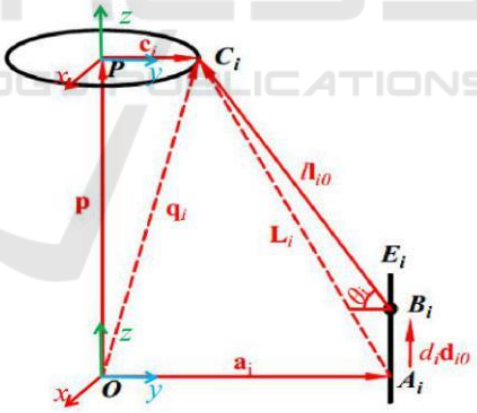

Figure 2. One limb of structure with coordinate systems of the platform.

Therefore, the displacement vector of the center of the moving platform in the moving frame P can be expressed as:

$$d_p = \left[p_x \; p_y \; p_z \; \alpha \; \beta \; \gamma \right]^T \tag{1}$$

Also, the position vectors of the S joints Ci (i=1, 2, 3) in P(xyz) frame can be defined by:

$$PC_1 = [r \;\; 0 \;\; 0]^{\mathrm{T}}$$
$$PC_2 = [-r/2 \;\; r\sqrt{3}/2 \;\; 0]^{\mathrm{T}} \quad (2)$$
$$PC_3 = [-r/2 \;\; -r\sqrt{3}/2 \;\; 0]^{\mathrm{T}}$$

Then, it is possible to obtain the rotation matrix T from the moving frame P(xyz) to the reference frame O(xyz), which can be expressed as:

$$T = R_x(\alpha) R_y(\beta) R_z(\gamma) = \begin{bmatrix} u_x & v_x & w_x \\ u_y & v_y & w_y \\ u_z & v_z & w_z \end{bmatrix} \quad (3)$$

The position vectors Ci (i=1,2,3) in the reference frame O can be defined by:

$$OC_i = OP + T \cdot PC_i \quad (4)$$

Substituting Eq.(2) and Eq.(3) into Eq.(4), we can obtain:

$$OC_1 = [p_x + u_x r \;\; p_y + u_y r \;\; p_z + u_z r]^T$$
$$OC_2 = [p_x - u_1 + v_1 \;\; p_y - u_2 + v_2 \;\; p_z - u_3 + v_3]^T \quad (5)$$
$$OC_3 = [p_x - u_1 - v_1 \;\; p_y - u_2 - v_2 \;\; p_z - u_3 - v_3]^T$$

Where $u_1 = \frac{u_x r}{2}$, $u_2 = \frac{u_y r}{2}$, $u_1 = \frac{u_z r}{2}$, $v_1 = \frac{\sqrt{3} u_x r}{2}$, $v_2 = \frac{\sqrt{3} u_y r}{2}$, $v_3 = \frac{\sqrt{3} u_z r}{2}$.

The position vectors of the R joints B_i $(i = 1,2,3)$ in O frame can be expressed as:

$$OB_1 = [R \;\; 0 \;\; d_1]^{\mathrm{T}}$$
$$OB_2 = [-R/2 \;\; R\sqrt{3}/2 \;\; d_2]^{\mathrm{T}} \quad (6)$$
$$OB_3 = [-R/2 \;\; -R\sqrt{3}/2 \;\; d_3]^{\mathrm{T}}$$

Where $d_i (i = 1,2,3)$ represented the translation of the passive joint.

Substituting Eq.(5) into Eq.(6) yields, the parasitic motions can be obtained:

$$\gamma = -\mathrm{atan}\left(\frac{s\alpha \; s\beta}{c\alpha + c\beta} \right) \quad (7)$$

$$p_x = \frac{r}{2}(c\beta \; c\gamma + s\alpha \; s\beta \; s\lambda - c\alpha \; c\gamma) \quad (8)$$

$$p_y = -\frac{r}{2}(c\alpha \; s\gamma + c\gamma \; s\alpha \; s\beta) \quad (9)$$

From the Figure 2, we can know the relation:

$$L_i = C_i B_i = OC_i - OB_i \quad (10)$$

Where OC_i and OB_i are expressed in Eq.(5) and Eq.(6).

Since $d_i (i = 1,2,3)$ is the only unknown variable in Eq.(6), solving Eq.(10) allows us to obtain the solutions for the inverse kinematic problem.

$$d_i = OC_{iz} \pm \sqrt{l^2 - (OB_{ix} - OC_{ix})^2 - (OB_{iy} - OC_{iy})^2} \quad (11)$$

4 SIMULATION RESULTS

4.1 Simulation Design of the Large-Stroke Flexure Joints

There are many types of flexible hinges. There are five common types: V-shaped, hyperbolic, parabolic, elliptical, and rounded straight beam flexible hinges, which correspond to 1~5 in Figure 3 below. For the same material, the same boundary and load conditions of 5N, the deformation and stress of the flexible hinges by ANSYS workbench were shown in Figure 4. The maximum displacement is in the order of: 5 > 4 > 3> 2> 1. The larger the maximum displacement of the flexible hinge, the more helpful it is to meet the large stroke requirement of the motion platform. By comparison, a rounded straight beam type flexible hinge has better structural characteristics and mechanical properties.

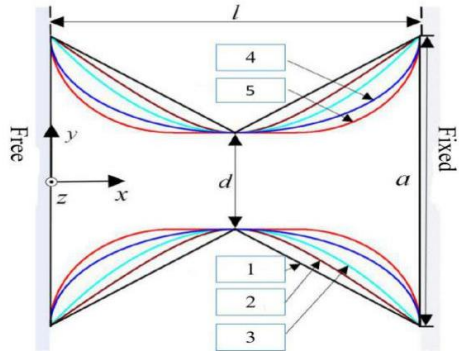

Figure 3. The section type of the flexible hinge.

A theoretical mechanical model is established for the flexible hinge, and the evaluation indexes includes rotational capacity θ and relative rotational error s, which can be seen in (Shi, et al., 2013).

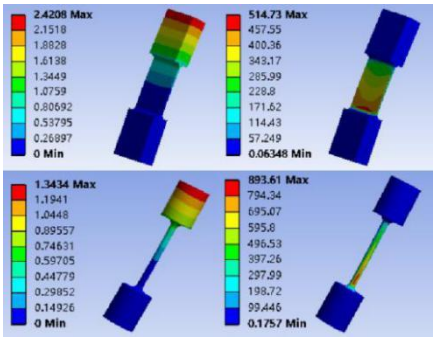

Figure 4. The deformation and stress of the flexible hinges.

It can be seen that the main parameters affecting the performance of the flexible spherical joint are: the length of the hinge deformation part L and the minimum diameter of the middle elongation t. A group of typical values L=12mm, t=1mm are selected, then change a variable near the typical value with other variables fixed , the data graphs of the influence on rotational capacity and relative rotational error are shown in Figure 5.

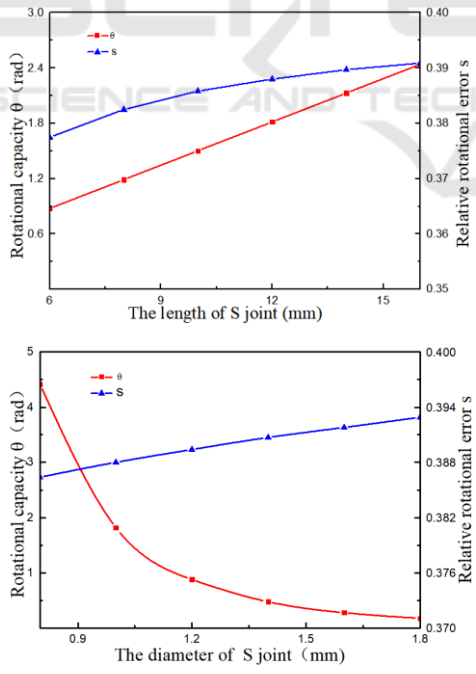

Figure 5. The performance of the flexible spherical joints in terms of L and t.

In the same way, the main parameters affecting the performance of the flexible revolute joint are the length L, the minimum thickness t, and the width b. A group of typical values L=12mm, t=0.4mm, and b=8mm were selected, and the data graphs of influence are shown in Fig 6.

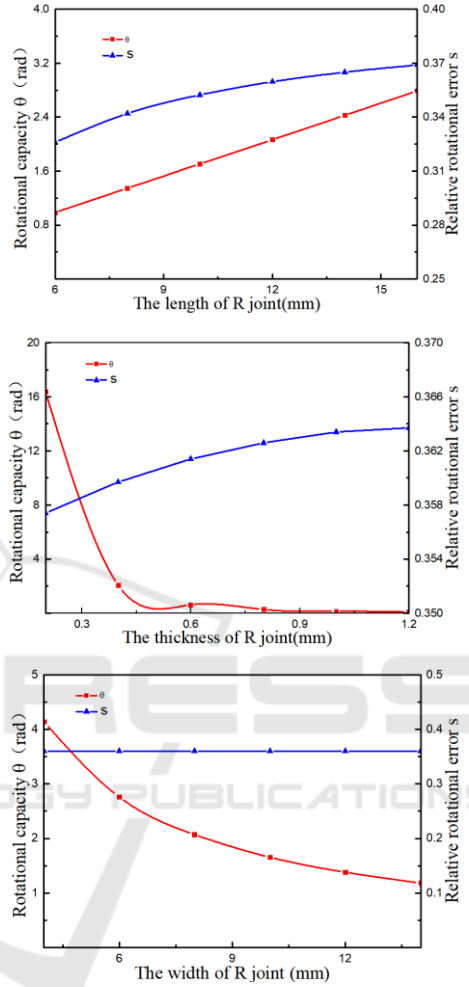

Figure 6. The performance of the flexible rotating joints in terms of L, t and b.

As shown in Figure 5 and Figure 6, with the increase of the length of the joints, the rotational capacity and the relative rotational error increased. The increase in the diameter of S joints, the thickness and width or R joints causes the increased rotational capacity and the educed relative rotational error. At the same time, the influence of the hinge size on the stiffness and stroke of the platform is also analyzed. The influence on the stroke of the platform and the law of the hinge size and the rotation ability are the same. By contrast, the influence on the stiffness of the platform is opposite to the rotation ability.

4.2 Inverse Kinematics Simulation

As shown in Table 2, the five pose values of the given platform are input into the pseudo rigid body kinematics model and the FEM model respectively to obtain the displacement of the driver. It can be seen from the above table that the results of Matlab and Ansys calculations are very small, the error is within 2%, which verifies the correctness of the kinematics model, and also shows that the flexible parallel motion platform is regarded as a rigid body under small deformation conditions. The feasibility of the analysis. And the motion range of the moving platform are in Table 3.

Table 2. Comparison of FEA and Theoretical analysis.

z,α,β (mm, °, °)	Theoretical d1,d2,d3 (mm,mm,mm)	FEM d1,d2,d3 (mm,mm,mm)
(5,0,0)	(5,5,5)	(5,5,5)
(0,0,0.5)	(-0.2373,0.1193, 0.1193)	(-0.2385,0.1208, 0.1207)
(0,0.5,0)	(-0.0001,0.2070, -0.2056)	(0.0005,0.2091, -0.2066)
(0,1,0.5)	(-0.2383,0.5355, -0.2931)	(-0.2367,0.5425, -0.2912)
(0.5,0.5,1)	(0.0264,0.9447, 0.5309)	(0.0262,0.9532, 0.5344)

Table 3. The motion range of the moving platform.

	Positive limit	Negative limit
Angular displacement around x axes(°)	9.2	-9.3
Angular displacement around y axes(°)	9	-9.5
Linear displacement along z axes(mm)	10	-10

4.3 Forward Kinematic Simulation

Given a trajectory of the platform, $\alpha = 0.5\sin(2\pi t)$, calculate the movements of the driving units by the FEA model and the inverse kinematic model. Then the values were employed to the forward kinematic model by FEA respectively. The movements in the actuator are shown in Figure 7, and the trajectory of the platform by theoretical modal and FEA modal are shown in Figure 8. The comparison between two models shows that the maximum positioning error is 0.0075 degrees in the range of 0.5 degrees. The results shows that the errors between two models are very small.

5 CONCLUSION

In this paper, a new 3-PRS compliant micro parallel platform with large-stroke hinges is presented. The platform is driven by a piezoelectric motor, and the

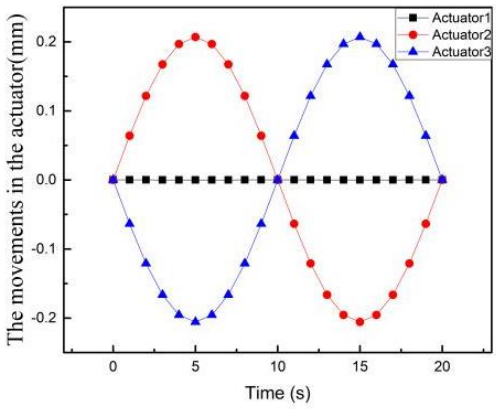

Figure 7. The movements of the actuators.

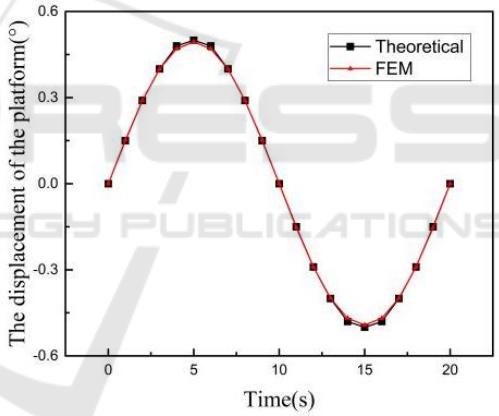

Figure 8. The end pose of the platform.

wide-range flexure hinges including spherical hinges and rotating hinges, which can improve the accuracy and increase travel. The FEA model of the large-stroke hinges are developed to analyze the characteristics and mechanical properties. Meanwhile, by using of the ANSYS Workbench, obtain the workspace of the manipulator, which can reach about 18° around x axes, 18° around y axes, more than 20mm along z axes depending on the travel of the drive part. An inverse kinematic solution is given, several comparison results between theoretical and simulation show that the model is effective for modeling compliant parallel platforms with wide-range flexible joints.

ACKNOWLEDGMENTS

This work was supported in part by the National Key Research and Development Program of China under Grant 2017YFB1104800, in part by the National Natural Science Foundation of China under Grant 51575534.

REFERENCES

Bhagat U, Shirinzadeh B, Clark L, et al. (2014). Design and analysis of a novel flexure-based 3-DOF mechanism. Mechanism & Machine Theory, 74(6):173-187.

Dong, W. Du, Z, and Sun, L. (2005). Stiffness influence atlases of a novel flexure hinge-based parallel mechanism with large workspace. IEEE/RSJ International Conference on Intelligent Robots & Systems. IEEE. Pages 856-861.

Gregorio, R. D., and Parenti-Castelli, V. (1998). A translational 3-DOF parallel manipulator. Advances in Robot Kinematics: Analysis and Control, Page 49–58.

Huang, S. C, and Dao, T. P. (2016). Design and computational optimization of a flexure-based xy positioning platform using fea-based response surface methodology. International Journal of Precision Engineering and Manufacturing, 17(8):1035-1048.

Jia, D. Y, Zhang, J. M., Niu, Z. G. et al. (2007). Inverse kinematics analysis and numerical control experiment for PRS-XY style hybrid machining tool. Frontiers of Mechanical Engineering, 2(2):235-238.

Li, Q. Chen, Z. Chen, Q. Wu, C. and Hu, X. (2011). Parasitic motion comparison of 3-PRS parallel mechanism with different limb arrangements. Robotics and Computer-Integrated Manufacturing, 27(2):389-396.

Liu, X. J, Tang, X., and Wang, J. (2005). Hana: a novel spatial parallel manipulator with one rotational and two translational degrees of freedom. Robotica, 23(2):257–70.

Li X, Zhu D, Mei Z, et al. (2017). Kinematic analysis of 3-RPS parallel mechanism.International Conference on Robotics and Automation Engineering. 2017:183-187.

Li, Y, and Xu, Q. (2007). Kinematic analysis of a 3-PRS parallel manipulator. Robotics and Computer-Integrated Manufacturing, 23(4):395-408.

Rouhani, E., and Nategh, M. J. (2016). An elastokinematic solution to the inverse kinematics of microhexapod manipulator with flexure joints of varying rotation center. Mechanism and Machine Theory, 97:127-140.

Ruiz, A, F. J. Campa, C. Roldán-Paraponiaris, Altuzarra, O, and Pinto, C. (2016). Experimental validation of the kinematic design of 3-PRS compliant parallel mechanisms. Mechatronics, 39:77-88.

Shi, R. C, Dong, W. and Du, Z. J. (2013). Design methodology and performance analysis of application-oriented flexure hinges. Review of Scientific Instruments, 84(7):065106.

Stewart, and D. (1965). A platform with six degrees of freedom. ARCHIVE: Proceedings of the Institution of Mechanical Engineers 1847-1982 (vols 1-196), 180(1965):371-386.

Tsai, M. S. Shiau, T. Tsai, Y. and Chang, T. (2003). Direct kinematic analysis of a 3-PRS parallel mechanism. Mechanism & Machine Theory, 38(1):71-83.

Wang, L. P, Xu, H. Y, et al. (2016). A novel 3-PUU parallel mechanism and its kinematic issues. Robotics and Computer-Integrated Manufacturing, 42:86-102.

Zhan, T. S, and Kao, C. C. (2010). Modified PSO method for robust control of 3RPS parallel manipulators. Mathematical Problems in Engineering, 2010(1):242-256.